Joint NICER/IXPE Workshop 2024

Discovery of Relativistic Disc-wind in X-ray Binaries for the 1st time: Wind-regulated accretion in 4U 1543-47

Geethu Prabhakar

Indian Institute of Space Science and Technology (IIST), Trivandrum

29 July 2024

OVERVIEW

- Introduction
- Comprehensive study using NICER
- Wideband Spectral Analysis
- Investigation of absorption feature
- Summary & Conclusion

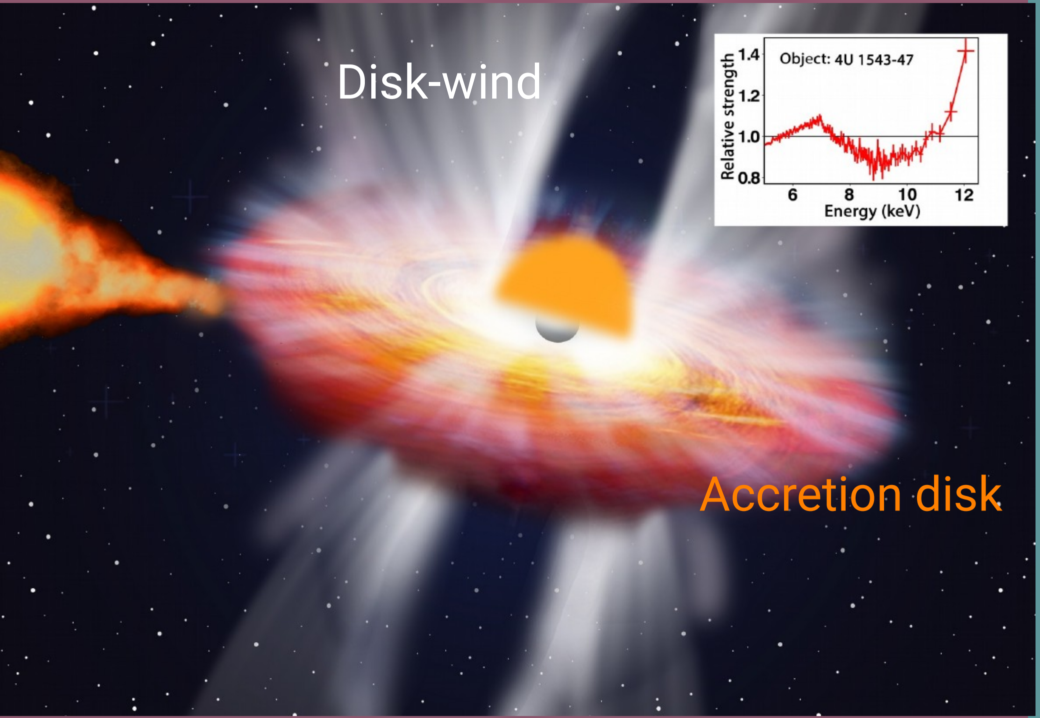


Monthly Notices of the ROYAL ASTRONOMICAL SOCIETY

MNRAS 520, 4889–4901 (2023)
Advance Access publication 2023 January 13

https://doi.org/10.1093/mnras/stad080

Wideband study of the brightest black hole X-ray binary 4U 1543–47 in the 2021 outburst: signature of disc-wind regulated accretion

Geethu Prabhakar,[1★] Samir Mandal,[1★] G. R. Bhuvana[2] and Anuj Nandi[3]
[1] Department of Earth and Space Sciences, Indian Institute of Space Science and Technology (IIST), Trivandrum 695547, India
[2] Department of Physics, Dayananda Sagar University, Bengaluru 560068, India
[3] Space Astronomy Group, ISITE Campus, U R Rao Satellite Centre, Bengaluru 560037, India

Accepted 2022 December 24. Received 2022 December 3; in original form 2022 October 25

ABSTRACT
A comprehensive wideband spectral analysis of the brightest black hole X-ray binary 4U 1543–47 during its 2021 outburst is carried out for the first time using *NICER*, *NuSTAR*, and *AstroSat* observations by phenomenological and reflection modelling. The source attains a super-Eddington peak luminosity and remains in the soft state, with a small fraction (< 3 per cent) of

4U 1543-47

THE ASTROPHYSICAL JOURNAL, 174:L53–L55, 1972 May 15
© 1972. The American Astronomical Society. All rights reserved. Printed in U.S.A.

A NEW TRANSIENT SOURCE OBSERVED BY *UHURU*

T. A. MATILSKY, R. GIACCONI, H. GURSKY, E. M. KELLOGG, AND H. D. TANANBAUM
American Science and Engineering, Cambridge, Massachusetts

Received 1972 March 27

ABSTRACT

A strong X-ray source appeared sometime between 1971 March 25 and 1971 August 17. On August 23, its intensity, as observed by the *Uhuru* satellite, was about twice that of the Crab Nebula, corresponding to about 3.0×10^{-8} ergs cm^{-2} s^{-1} in the range 2–6 keV. On 1971 December 20, its intensity had declined to one-tenth of that value in the same energy range. Its spectrum was quite steep, and fit a power law with an average energy spectral index of 3.0. The variation of X-ray intensity over a 5-month period shows qualitative differences from the previously observed transient X-ray sources, Cen XR-2 and Cen XR-4.

- Discovered by Uhuru satellite on 1971
- Subsequent outbursts : 1984, 1992, 2002, 2021
- RA = 15h 47m 8.27s, DEC = −47°40'10.8" (J2000)
- The **brightest XRB** source ever discovered :

  11.6 Crab in 2−4 keV (2021 outburst)
- Distance : D = 7.5 ± 0.5 kpc (Jonker & Nelemans 2004)
- Mass of the black hole : M = 9.4±1 $M_{\odot}$ (Russell et al. 2006)
- Low orbital inclination

Lightcurve and Hardness ratio

Extremely luminous
in low energies

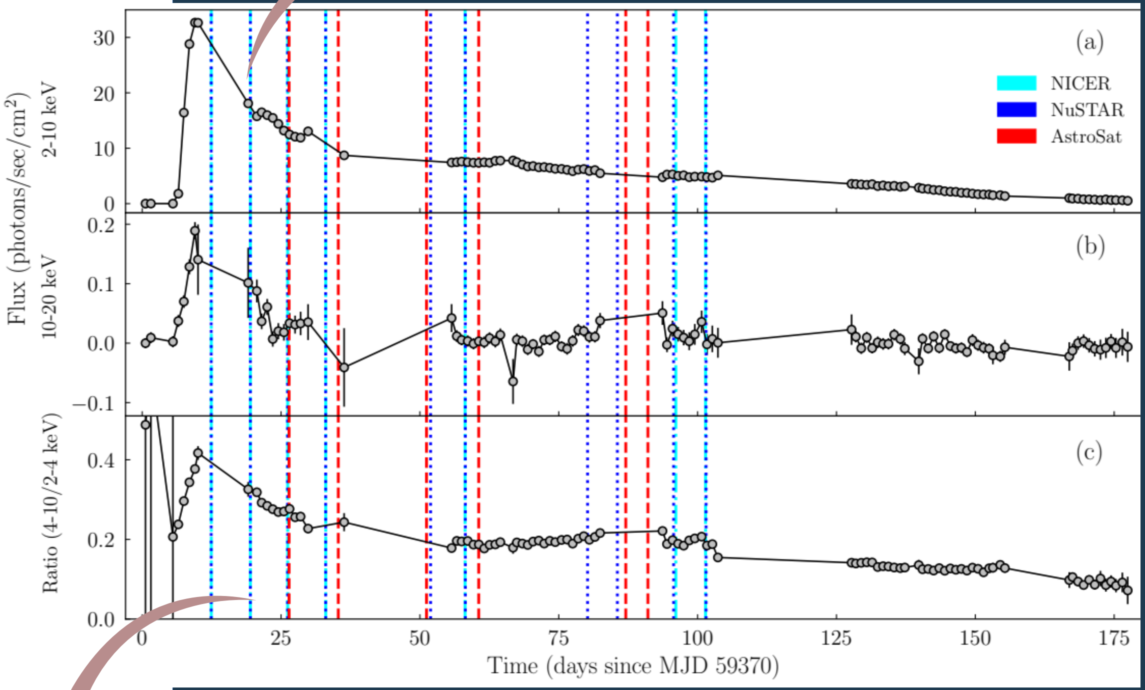

HR evolution

MAXI lightcurve

(Prabhakar et al. 2023)

Lightcurve and Hardness ratio

Extremely luminous
in low energies

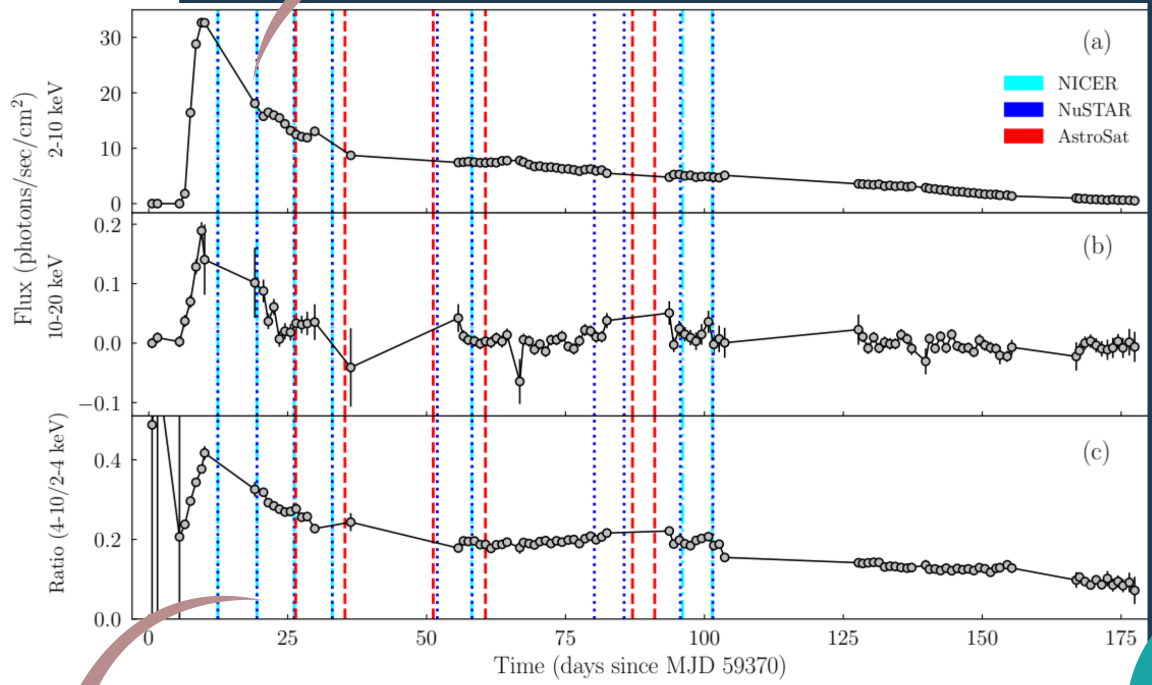

HR evolution

MAXI lightcurve

Mostly
in HSS

(Prabhakar et al. 2023)

Lightcurve and Hardness ratio

Extremely luminous
in low energies

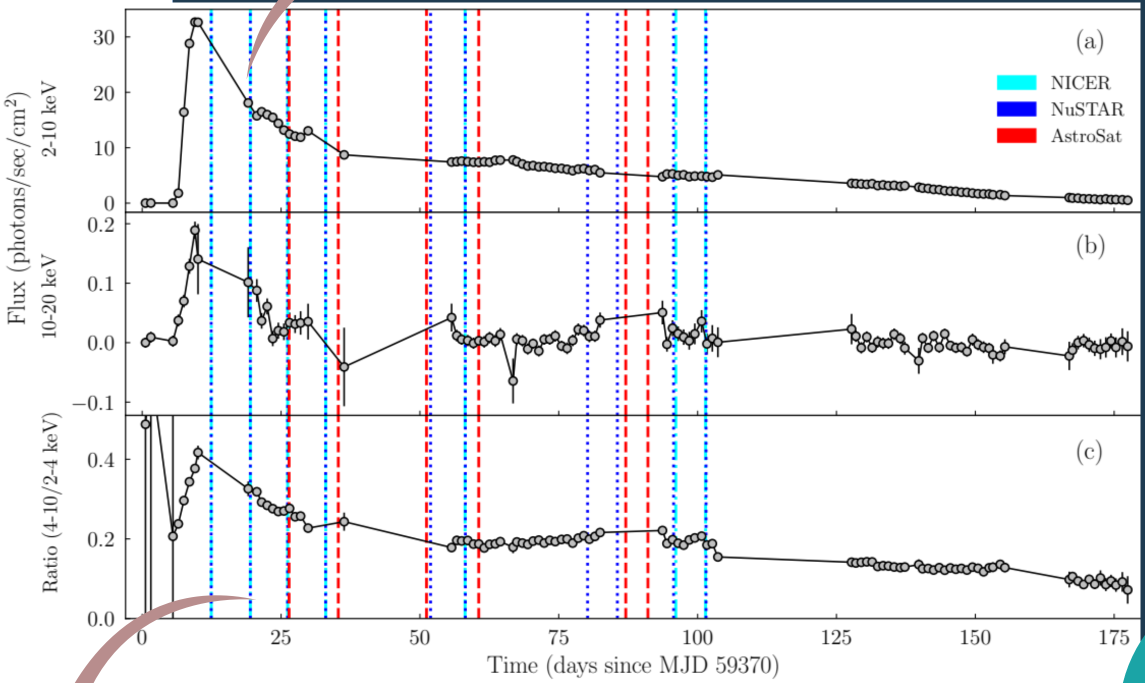

HR evolution

MAXI lightcurve

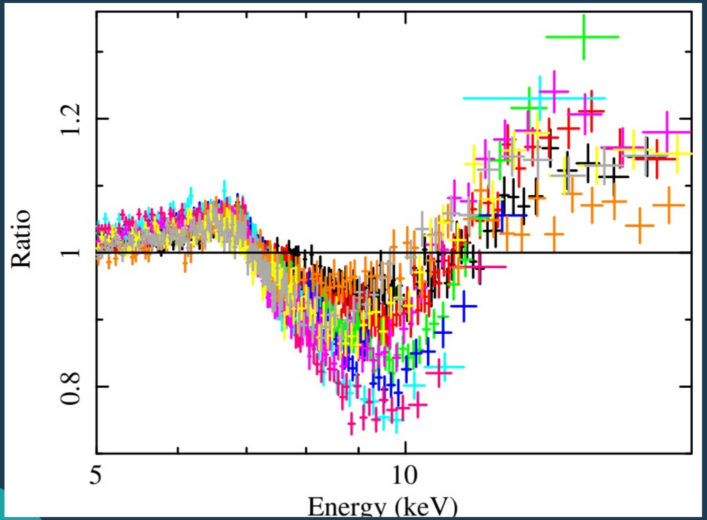

NuSTAR : tbabs(diskbb+powerlaw)

Mostly
in HSS

(Prabhakar et al. 2023)

Lightcurve and Hardness ratio

Extremely luminous
in low energies

Very strong
absorption feature !

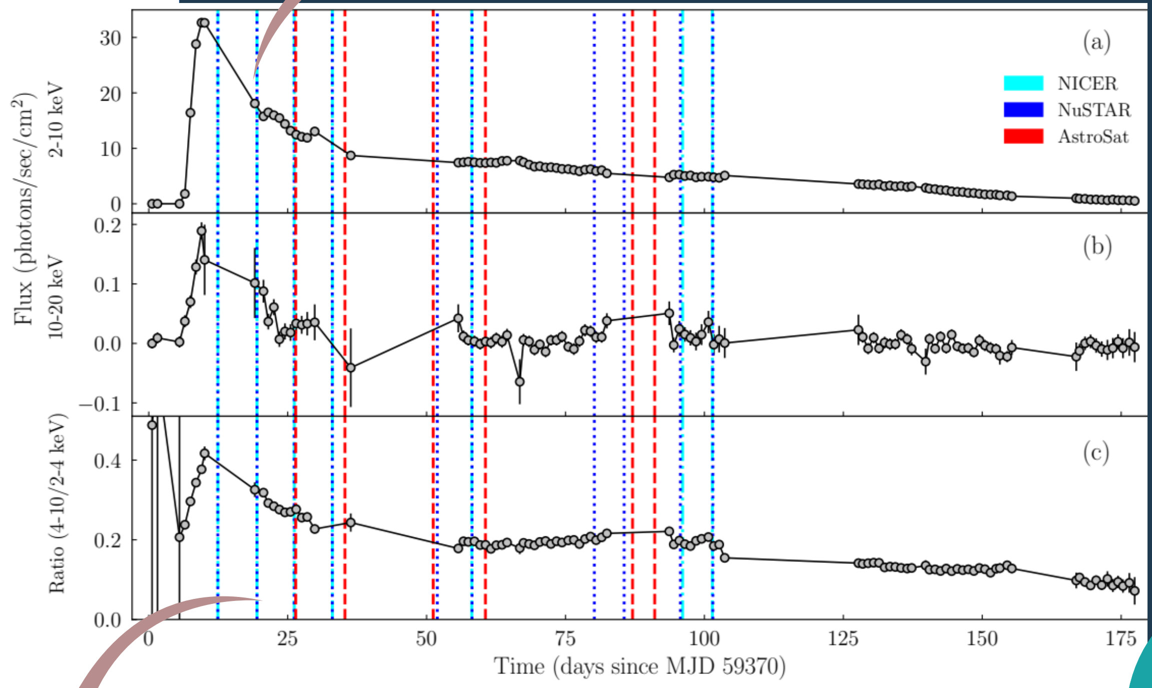

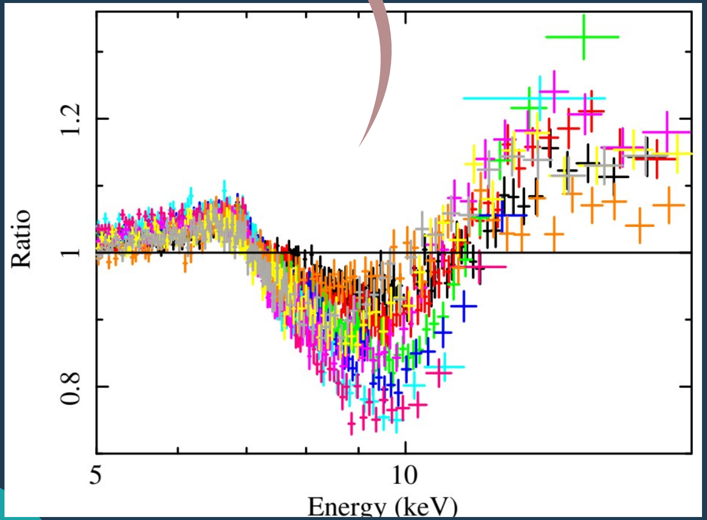

NuSTAR : tbabs(diskbb+powerlaw)

Mostly
in HSS

HR evolution

MAXI lightcurve

(Prabhakar et al. 2023)

Lightcurve and Hardness ratio

Extremely luminous
in low energies

Very strong
absorption feature !

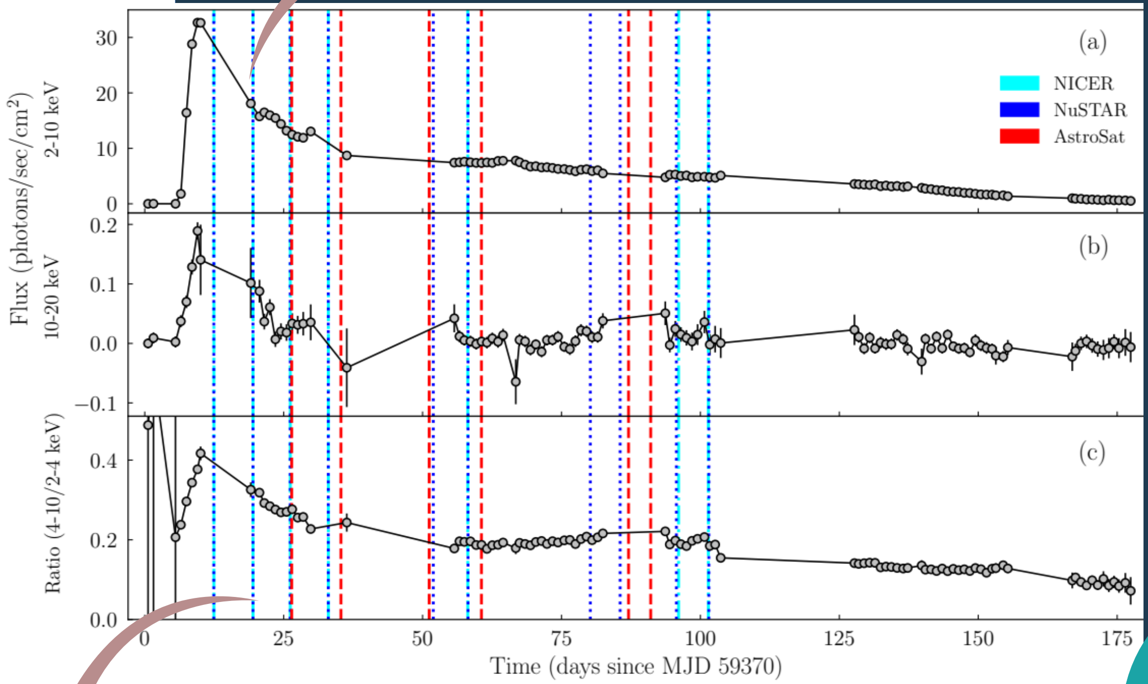

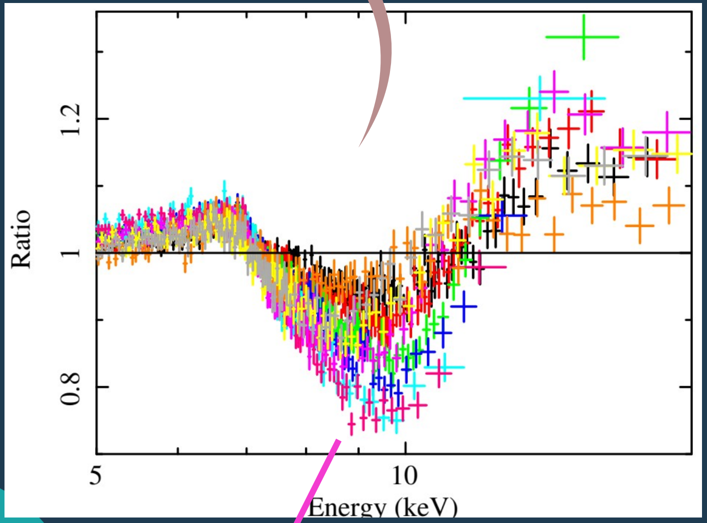

NuSTAR : tbabs(diskbb+powerlaw)

HR evolution

MAXI lightcurve

Mostly
in HSS

Maximum on ~day 60

(Prabhakar et al. 2023)

MOTIVATION

There is no comprehensive study in literature based on 2021 outburst of 4U 1543−47.

We noticed extreamly strong and dynamic absorption features in the 2021 outburst spectra: has not been observed in XRBs.

Find out the origin of this unique absorption feature and understand its role in accretion.

Comprehensive Study of the Outburst

- Hardness Intensity Diagram -

NICER

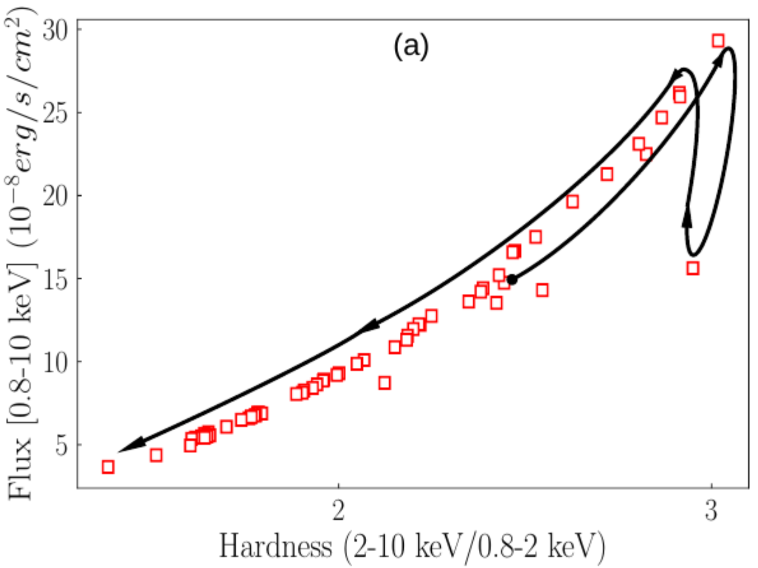

Wideband Spectral Analysis

Phenomenological Modelling

- For Comptonized spectrum: ***thcomp***
- For strong absorption feature : ***gabs***
- For weak Fe Kα absorption edge : ***edge***

NICER-NuSTAR

0.8 – 10 keV & 4 – 60 keV

tbabs(thcomp × diskbb)edge × gabs

AstroSat

0.5 – 7 keV & 3 – 30 keV

tbabs(thcomp × diskbb) gabs

Model M1

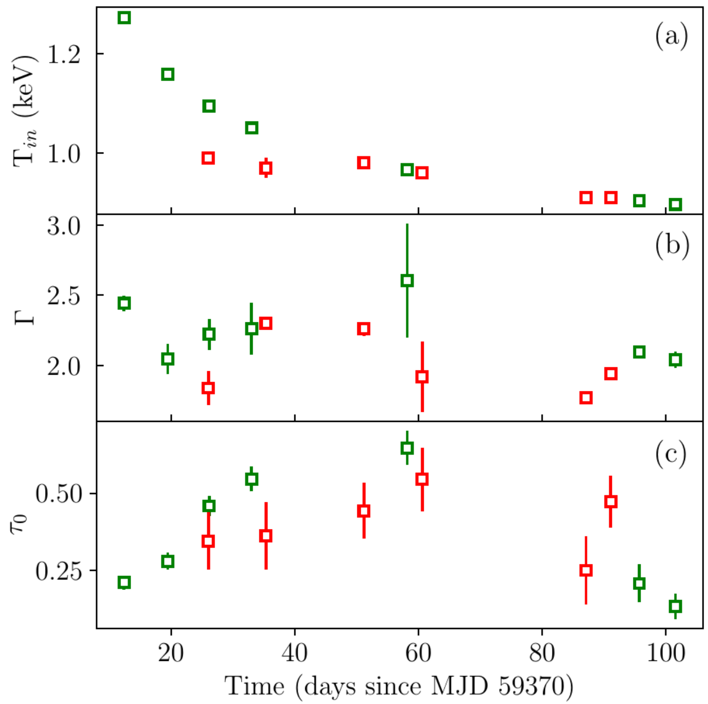

Phenomenological modelling

- Evolution of Parameters -

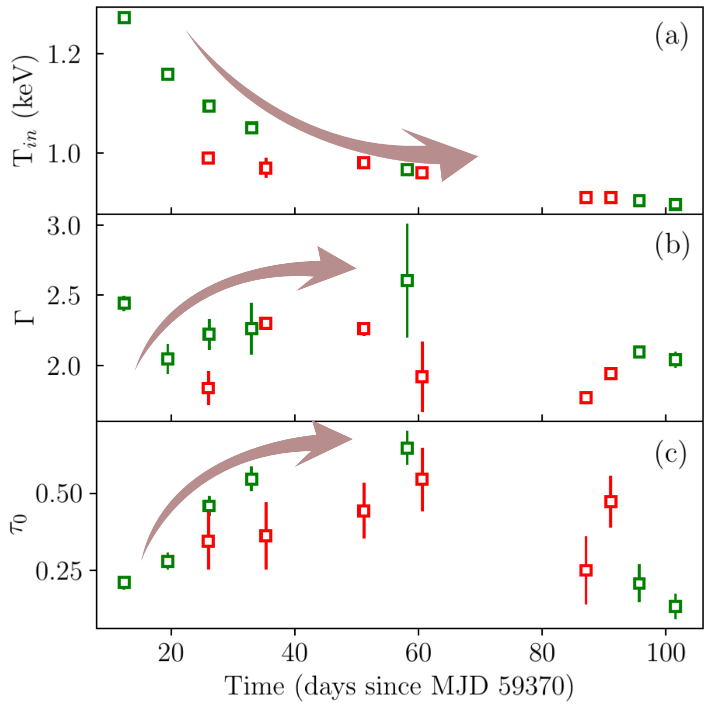

Phenomenological modelling

- Evolution of Parameters -

T_{in} decreases throughout the outburst decay.

Γ : increases till ~day 60, then decreases.

f_c : decreases till ~day 60 then increases - behaviour is consistent with the spectral softening trend. Only a tiny fraction (< 3 %) of the soft photons Comptonized in the corona.

Strength : increases till ~day 60: dynamic

Optical depth associated with *gabs*,

$\tau_0 = strength / \sigma \sqrt{2\pi}$

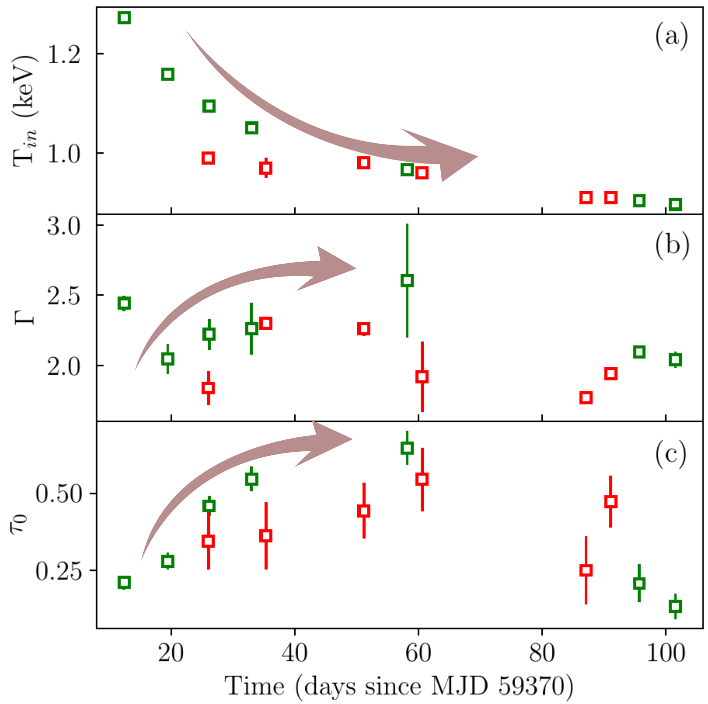

Phenomenological modelling

- Evolution of Parameters -

T_{in} decreases throughout the outburst decay.

Γ : increases till ~day 60, then decreases.

f_c : decreases till ~day 60 then increases - behaviour is consistent with the spectral softening trend. Only a tiny fraction (< 3 %) of the soft photons Comptonized in the corona.

Strength : increases till ~day 60: dynamic

Optical depth associated with *gabs*,

τ_0 = *strength* /σ √2π

Luminosity exceeds L_{Edd} for the peak, then declines

Wideband Spectral Analysis

Reflection Modelling (RELXILL)

- **relxilllp**: powerlaw photons from corona with a high-energy cutoff illuminate the disk and reflected
- For strong absorption feature : ***gabs***

NICER-NuSTAR

0.8 – 10 keV & 4 – 60 keV

AstroSat

0.5 – 7 keV & 3 – 30 keV

tbabs(diskbb+relxilllp)gabs

Model M2

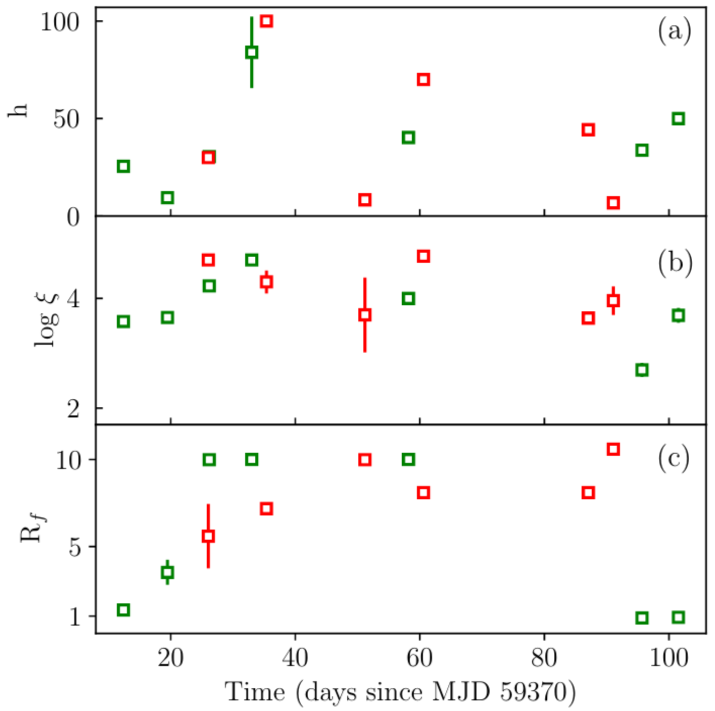

Reflection modelling

- Evolution of Parameters -

T_{in} and Γ - silimlar trend of evolution as in M1

Inclination θ ~ 32°-40°

High value of log ξ (>3) : a highly ionized disc material throughout the outburst

Overabundance (3.6 – 10 $A_{Fe,\odot}$) of iron in the disk.

R_f : The fraction of primary photons reaching the disk increases till ~day 60, then decreases afterwards.

gabs strength estimated from both methods follow the same trend

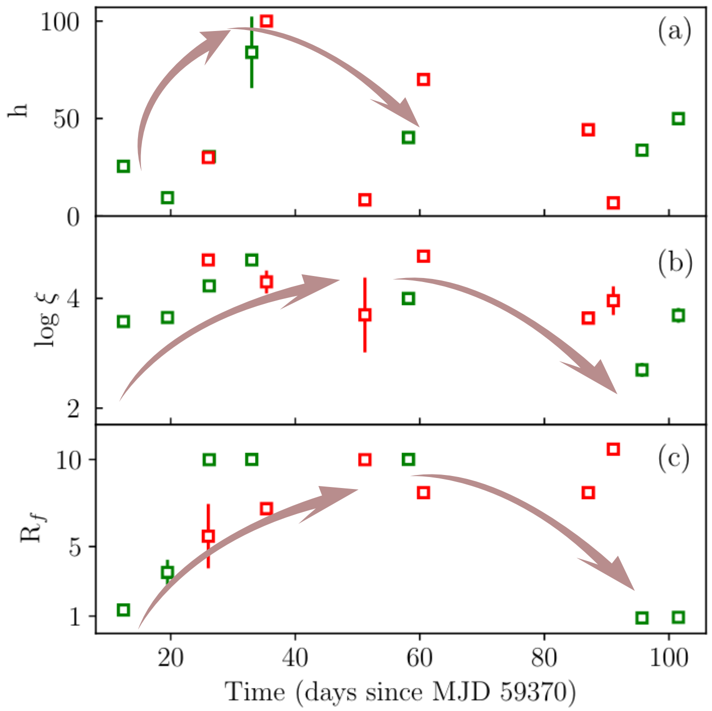

Reflection modelling

- Evolution of Parameters -

T_{in} and Γ - silimlar trend of evolution as in M1

Inclination θ ~ 32°-40°

High value of log ξ (>3) : a highly ionized disc material throughout the outburst

Overabundance (3.6 – 10 $A_{Fe,\odot}$) of iron in the disk.

R_f : The fraction of primary photons reaching the disk increases till ~day 60, then decreases afterwards.

gabs strength estimated from both methods follow the same trend

Investigation of the Absorption feature

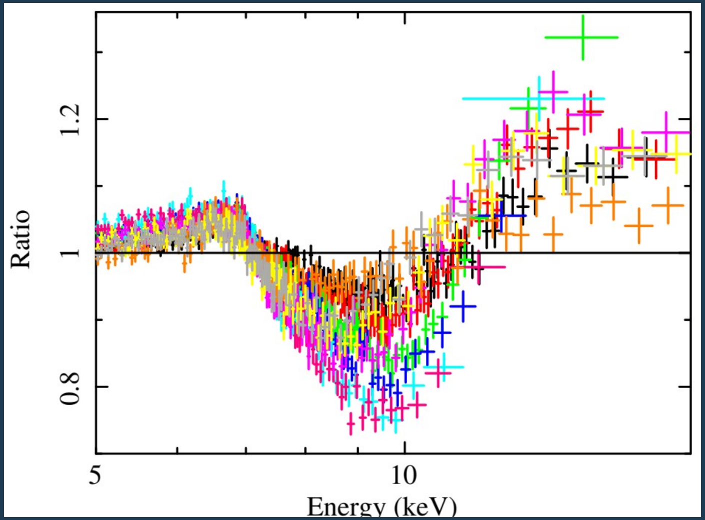

Absorption features in the Spectra of 4U 1543−47

..can be due to

- Obscuring cloud in the line-of-sight
- Occultation due to companion star
- Stellar wind from companion
- Strong accretion disk-wind

Absorption features in the Spectra of 4U 1543−47

..can be due to

- Obscuring cloud in the line-of-sight
- Occultation due to companion star
- Stellar wind from companion
- Strong accretion disk-wind

Absorption features in the Spectra of 4U 1543−47

..can be due to

- Obscuring cloud in the line-of-sight
- Occultation due to companion star
- Stellar wind from companion
- Strong accretion disk-wind

Used partial covering fraction model *(pcfabs)*

Absorption features in the Spectra of 4U 1543−47

..can be due to

- Obscuring cloud in the line-of-sight ✗
- Occultation due to companion star
- Stellar wind from companion
- Strong accretion disk-wind

Used partial covering fraction model (*pcfabs*)

↓

No improvement in the fitting

Absorption features in the Spectra of 4U 1543−47

..can be due to

- Obscuring cloud in the line-of-sight ✗
- Occultation due to companion star
- Stellar wind from companion
- Strong accretion disk-wind

Used partial covering fraction model (*pcfabs*)

↓

No improvement in the fitting

Absorption features in the Spectra of 4U 1543−47

..can be due to

- Obscuring cloud in the line-of-sight ✕
- Occultation due to companion star
- Stellar wind from companion
- Strong accretion disk-wind

Used partial covering fraction model (*pcfabs*)

↓

No improvement in the fitting

Absorption features in the Spectra of 4U 1543−47

..can be due to

- Obscuring cloud in the line-of-sight ✕
- Occultation due to companion star
- Stellar wind from companion
- Strong accretion disk-wind

Used partial covering fraction model (*pcfabs*)

↓

No improvement in the fitting

→ Checking for orbital variations

Orbital variations ?

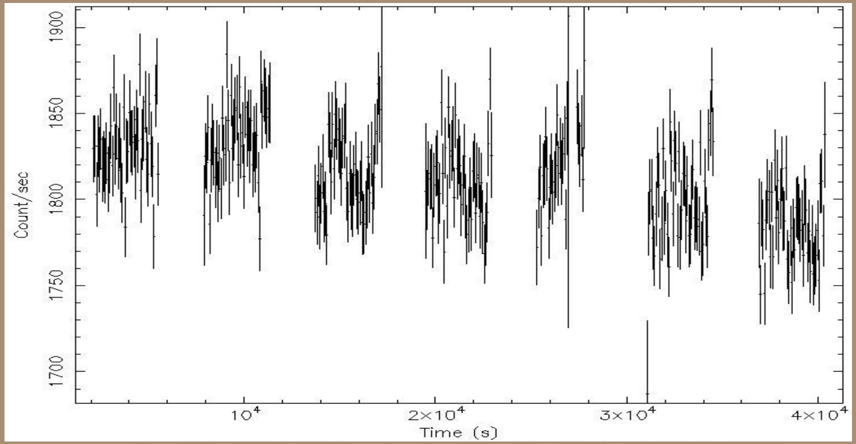

S_i

- All NuSTAR epoch data fitted using M1 and M2
- Estimated *gabs-strength* (S_i)

S_p

- Extracted spectrum from different patches of GTIs
- Simultaneous joint fit of all GTI-patches under each epoch using M1
- Estimated *gabs-strength* (S_p)

- **Binary orbital period 26.79 h**
- **The orbital position of each patch is identified based on the start time of Epoch -1**
- **Plotted S_p-S_i against orbital phase**
- **Residual varies within ±0.5 keV**

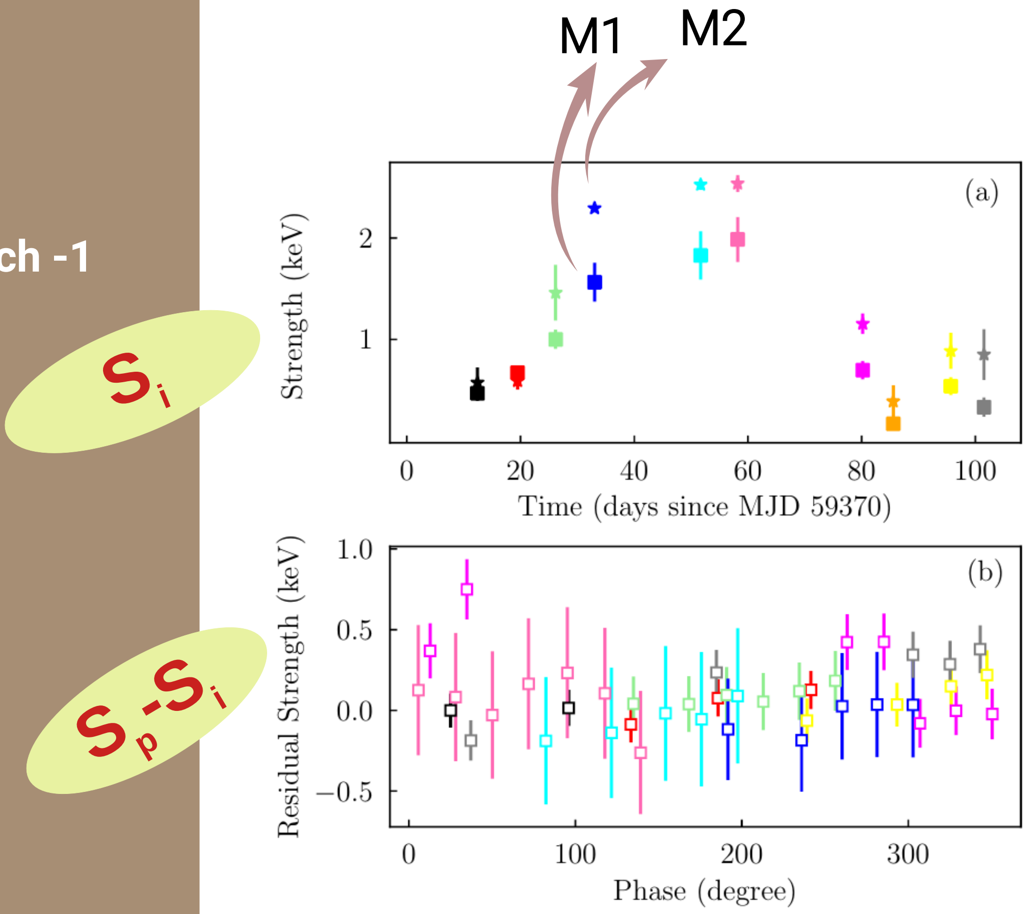

Residual strength (S_p - S_i) is measured for each patches inside an epoch

- **Binary orbital period 26.79 h**
- **The orbital position of each patch is identified based on the start time of Epoch -1**
- **Plotted S_p-S_i against orbital phase**
- **Residual varies within ±0.5 keV**

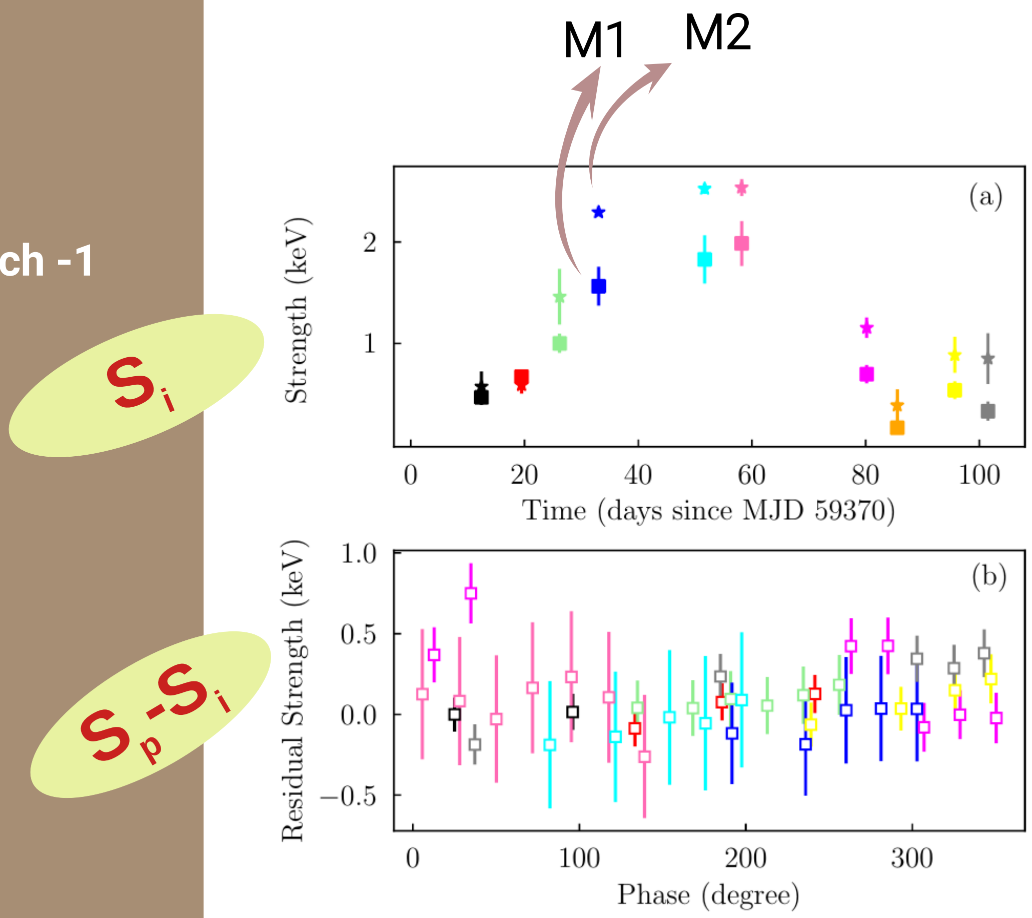

Residual strength (S_p - S_i) is measured for each patches inside an epoch

- **Binary orbital period 26.79 h**
- **The orbital position of each patch is identified based on the start time of Epoch -1**
- **Plotted S_p-S_i against orbital phase**
- **Residual varies within ±0.5 keV**

Orbital position of BH and companion is not responsible for the dynamic nature of the absorption features

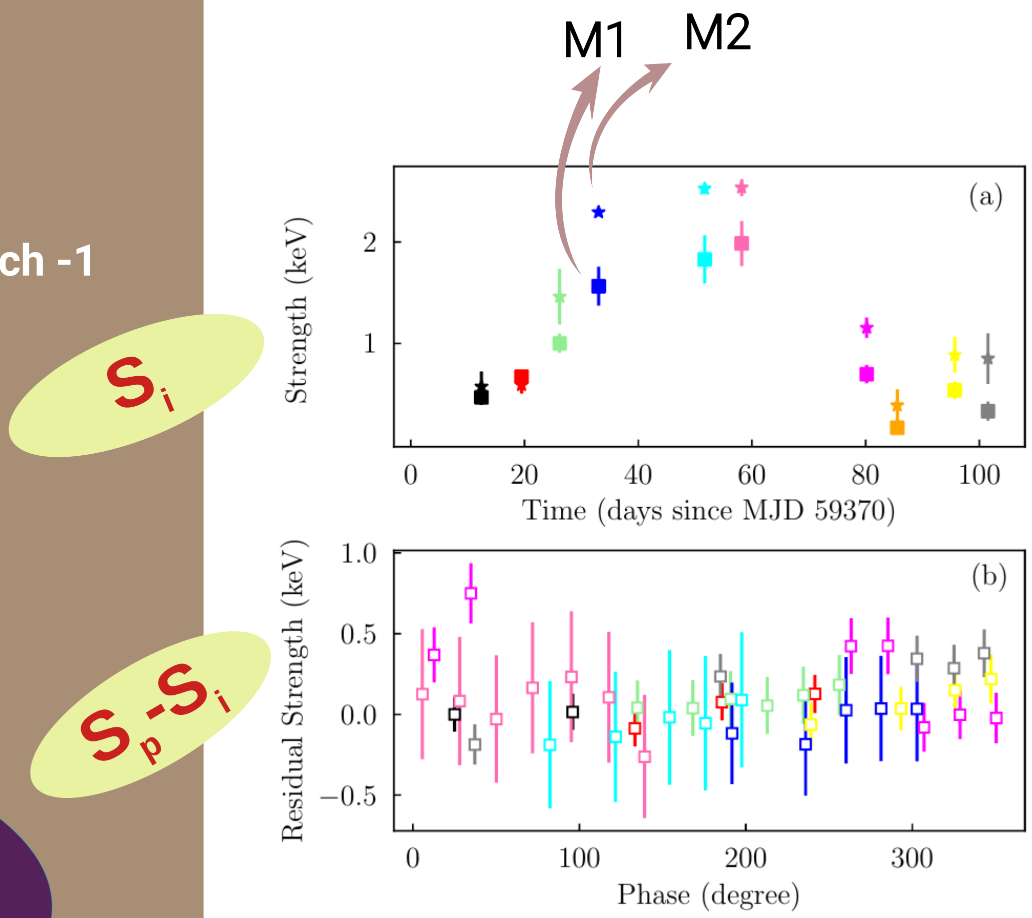

Residual strength (S_p - S_i) is measured for each patches inside an epoch

Absorption features

..can be due to

- Obscuring cloud in the line-of-sight ✕
- Occultation due to companion star ✕
- Stellar wind from companion
- Strong accretion disk-wind

Absorption features

..can be due to

- Obscuring cloud in the line-of-sight ✗
- Occultation due to companion star ✗
- Stellar wind from companion
- Strong accretion disk-wind

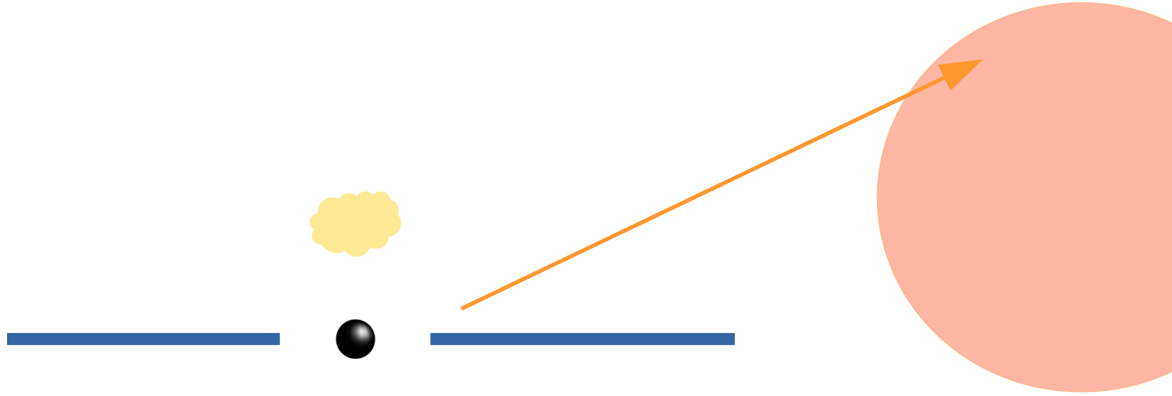

Absorption features

..can be due to

- Obscuring cloud in the line-of-sight ✕
- Occultation due to companion star ✕
- Stellar wind from companion
- Strong accretion disk-wind

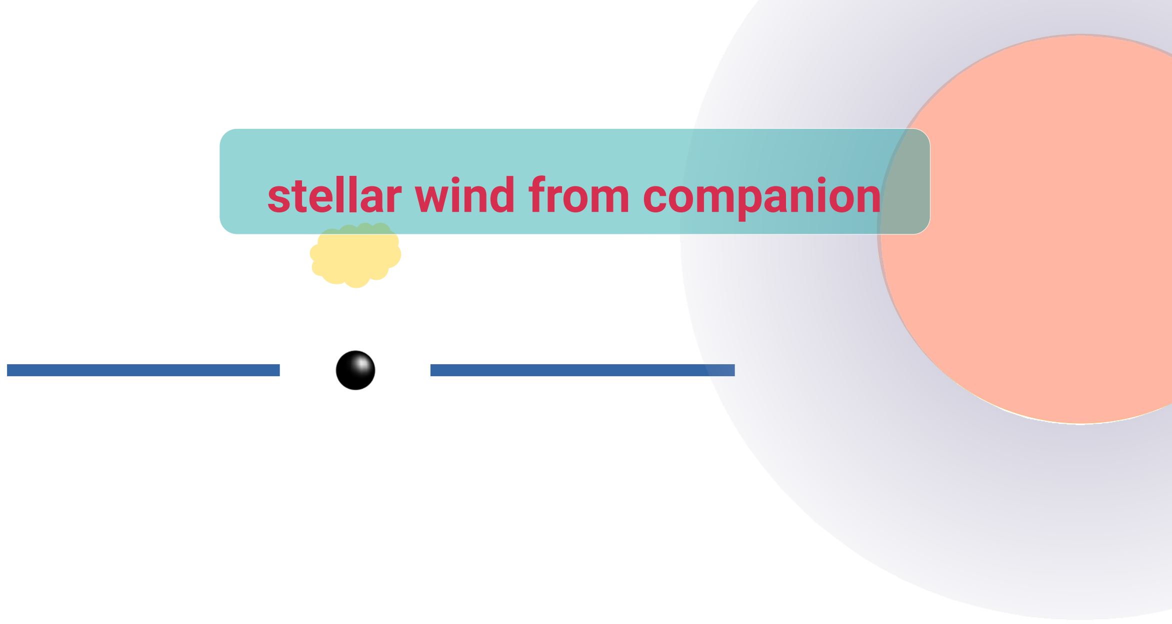

Absorption features

..can be due to

- Obscuring cloud in the line-of-sight ✗
- Occultation due to companion star ✗
- Stellar wind from companion
- Strong accretion disk-wind

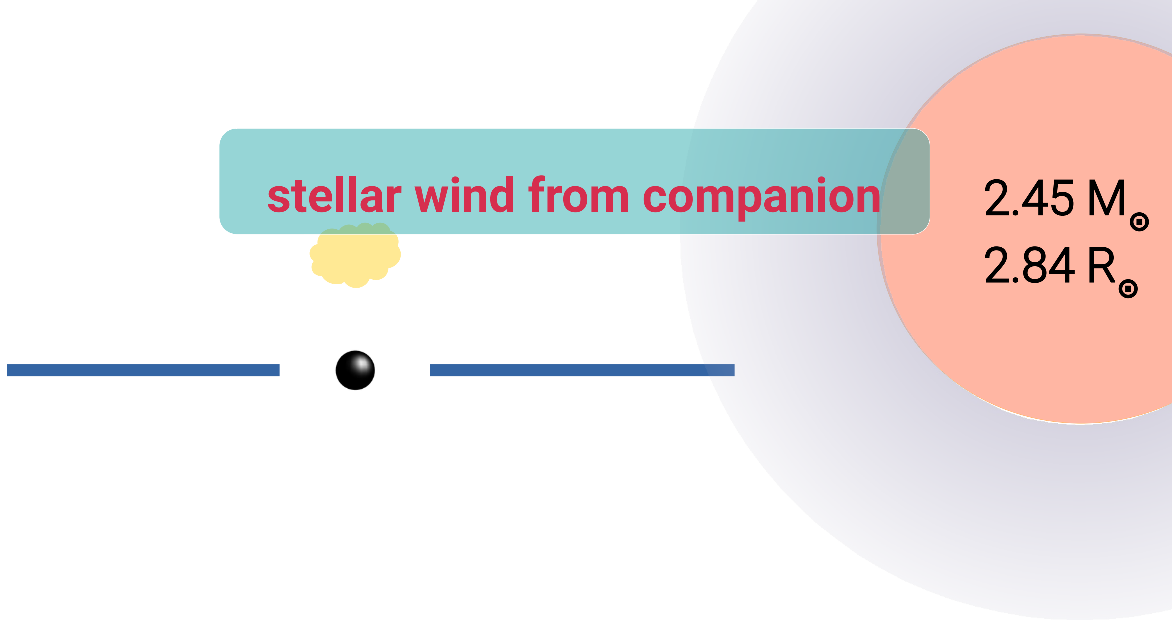

Absorption features

..can be due to

- Obscuring cloud in the line-of-sight ✕
- Occultation due to companion star ✕
- Stellar wind from companion
- Strong accretion disk-wind

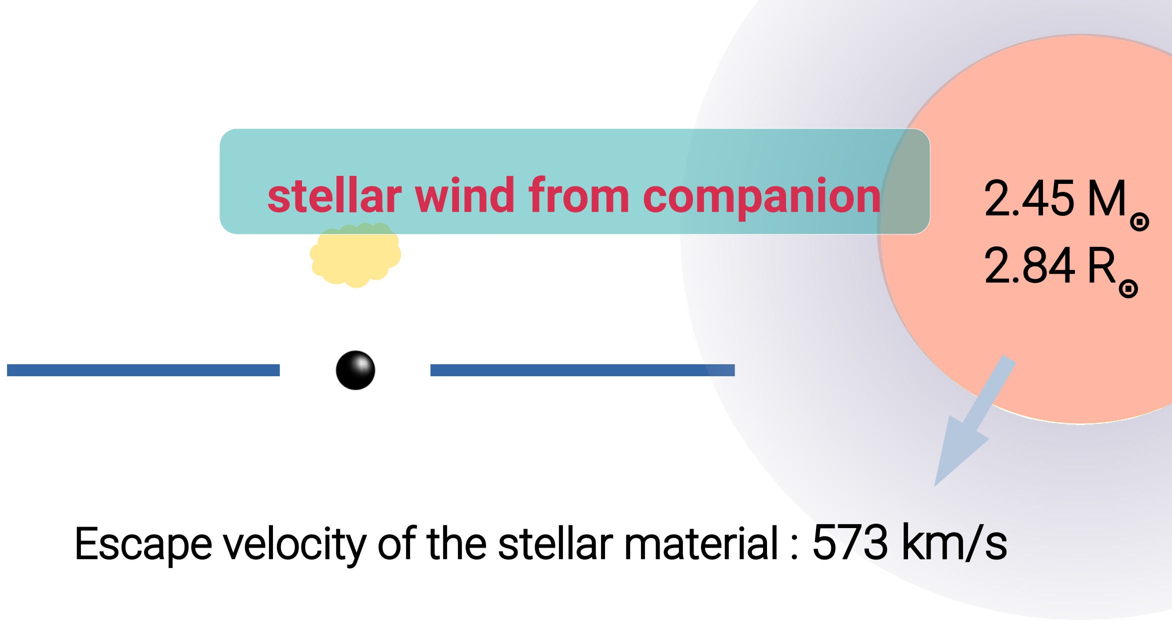

Escape velocity of the stellar material : 573 km/s

Absorption features

..can be due to

- Obscuring cloud in the line-of-sight ✗
- Occultation due to companion star ✗
- Stellar wind from companion
- Strong accretion disk-wind

Escape velocity of the stellar material : 573 km/s

Absorption features

..can be due to

- Obscuring cloud in the line-of-sight ✗
- Occultation due to companion star ✗
- Stellar wind from companion
- Strong accretion disk-wind

Escape velocity of the stellar material : 573 km/s

Stellar wind column density and ionization should decrease with X-ray luminosity, therefore absorption strength also

Absorption features

..can be due to

- Obscuring cloud in the line-of-sight ✗
- Occultation due to companion star ✗
- Stellar wind from companion ✗
- Strong accretion disk-wind

Escape velocity of the stellar material : 573 km/s

Stellar wind column density and ionization should decrease with X-ray luminosity, therefore absorption strength also

Absorption features

..can be due to

- Obscuring cloud in the line-of-sight ✗
- Occultation due to companion star ✗
- Stellar wind from companion ✗
- Strong accretion disk-wind

Accretion disk-wind

Super Eddington peak luminosity of the source can launch strong disk-wind

- **Disk-wind is more prominent in the soft state of XRB**
- **If the disk-ionized winds are responsible for the absorption features,**

expect maximum strength for the features when the source is softer : ~ day 60

Absorption features

..can be due to

- Obscuring cloud in the line-of-sight ✗
- Occultation due to companion star ✗
- Stellar wind from companion ✗
- Strong accretion disk-wind

Accretion disk-wind

Super Eddington peak luminosity of the source can launch strong disk-wind

- **Disk-wind is more prominent in the soft state of XRB**
- **If the disk-ionized winds are responsible for the absorption features,**

expect maximum strength for the features when the source is softer : ~ day 60

Absorption features

..can be due to

- Obscuring cloud in the line-of-sight ✗
- Occultation due to companion star ✗
- Stellar wind from companion ✗
- Strong accretion disk-wind

Accretion disk-wind

Super Eddington peak luminosity of the source can launch strong **disk-wind**

- Disk-wind is more prominent in the **soft state** of XRB
- If the disk-ionized winds are responsible for the absorption features,

expect maximum strength for the features when the source is softer : ~ **day 60**

Strength of absorption & optical depth are maximum on ~ day 60

Absorption features

..can be due to

- Obscuring cloud in the line-of-sight ✗
- Occultation due to companion star ✗
- Stellar wind from companion ✗
- Strong accretion disk-wind ●

Accretion disk-wind

Super Eddington peak luminosity of the source can launch strong disk-wind

- **Disk-wind is more prominent in the soft state of XRB**
- **If the disk-ionized winds are responsible for the absorption features,**

expect maximum strength for the features when the source is softer : ~ day 60

↓

Strength of absorption & optical depth are maximum on ~ day 60

- Transition energy of the most ionized line with the highest absorption yield (Fe XXV and Fe XXVI) : 6.68 and 6.97 keV
- Assuming the feature is produced by absorption of the accretion disk photons by highly ionized blue shifted disk-wind,

Estimated wind speed →

- Broad feature can be produced by combining multiple lines of various ionization states of iron.

- Transition energy of the most ionized line with the highest absorption yield (Fe XXV and Fe XXVI) : 6.68 and 6.97 keV
- Assuming the feature is produced by absorption of the accretion disk photons by highly ionized blue shifted disk-wind,

Estimated wind speed → **~30% of c**

- Broad feature can be produced by combining multiple lines of various ionization states of iron.

- Transition energy of the most ionized line with the highest absorption yield (Fe XXV and Fe XXVI) : 6.68 and 6.97 keV
- Assuming the feature is produced by absorption of the accretion disk photons by highly ionized blue shifted disk-wind,

Estimated wind speed → **~30% of c**

- Broad feature can be produced by combining multiple lines of various ionization states of iron.

1st relativistic disk-wind in XRBs!

Equivalent width evolution

- Phenomenological modelling shows the presence of the neutral Fe Kα absorption (edge) at ~ 7.1 – 7.4 keV (from outer disk)

- Once the luminosity reduces, there is a sudden infall of matter onto the BH, leading to an evacuation of the inner disk.

- Sudden drop of ionized EW (BC) can be due to the evacuation of the inner disk.

Highly luminous inner disk

Disk-wind maximum

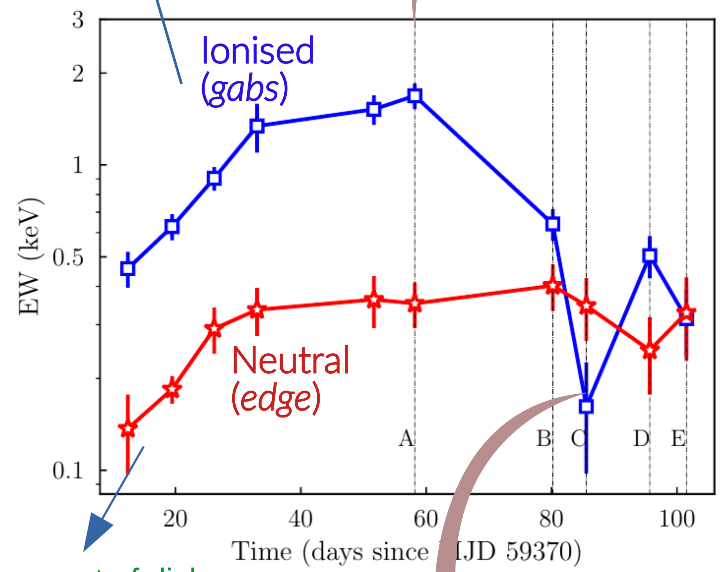

Enhancement of disk matter due to irradiation of the outer disk

Significant reduction in disk luminosity

Inner disk matter lost : Evacuation

Equivalent width evolution

- If evacuation happens → drop of soft photon flux

  Expect relatively harder spectrum

  Observed drop (14%) in soft flux (0.5-7 keV)

- Inner accretion disk recovers over the next 10 days (CD) due to transfer of matter from the outer disk

- Neutral component (or the outer disk) follows the same trend as the ionized component with a delay of the viscous timescale

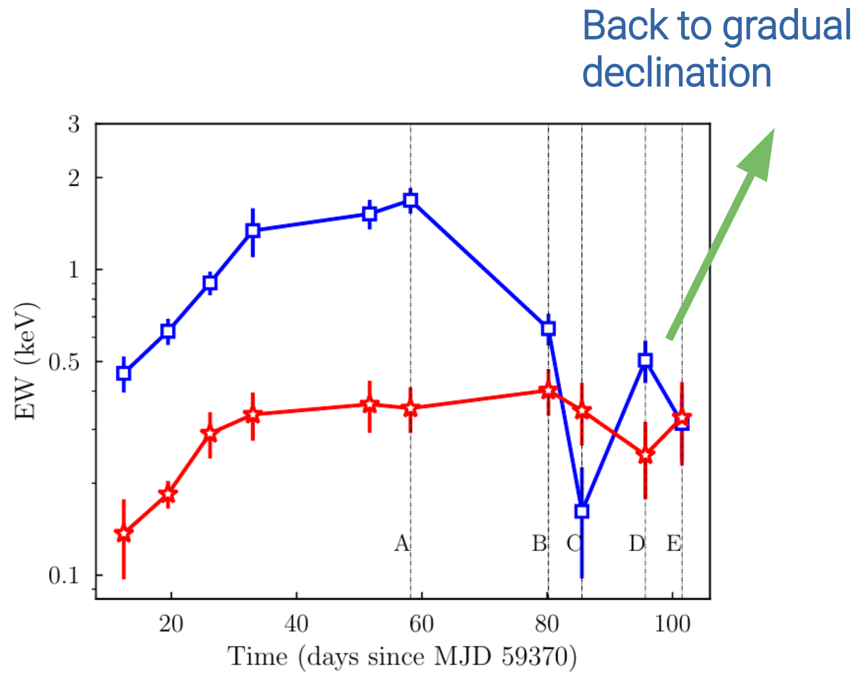

Equivalent width evolution

- If evacuation happens → drop of soft photon flux

  Expect relatively harder spectrum

  Observed drop (14%) in soft flux (0.5-7 keV)

- Inner accretion disk recovers over the next 10 days (CD) due to transfer of matter from the outer disk

- Neutral component (or the outer disk) follows the same trend as the ionized component with a delay of the viscous timescale

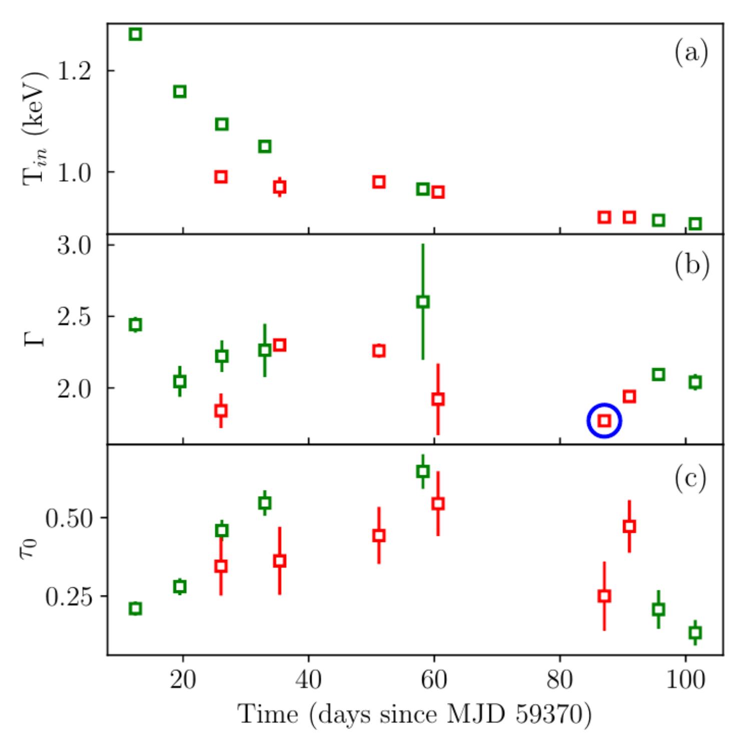

radual
on

Equivalent width evolution

- If evacuation happens → drop of soft photon flux

  Expect relatively harder spectrum

  Observed drop (14%) in soft flux (0.5-7 keV)

- Inner accretion disk recovers over the next 10 days (CD) due to transfer of matter from the outer disk

- Neutral component (or the outer disk) follows the same trend as the ionized component with a delay of the viscous timescale

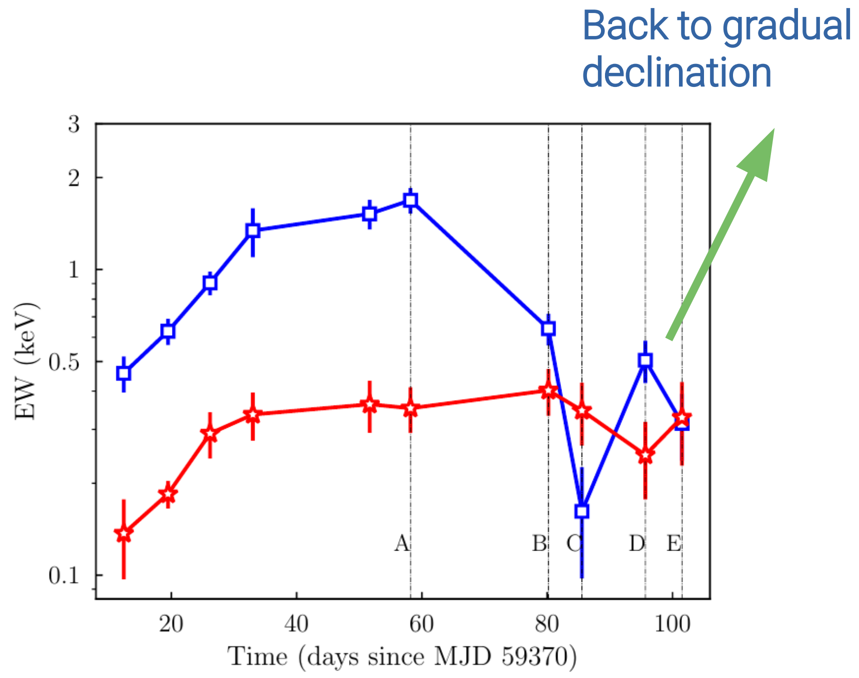

Summary & Conclusion

- Exhibit super Eddington peak luminosity on Epoch 1.
- Source is in HSS through out, with a steep Γ due to a very small fraction (< 3%) of inverse-Comptonized photons and low corona temperature.
- Inclination of the system ~$32^\circ - 40^\circ$
- Extreme luminosity, high ionization ($\log \xi > 3$) and overabundance of iron.
- HID : correlated evolution of flux and HR (thermal disc origin)
- A broad, dynamic absorption feature at $\sim 8 - 11$ keV : 1st time in XRBs. We propose that this feature is due to the absorption of the accretion disk photons by the highly ionized, blue shifted disk-wind.
- Estimated wind speed of nearly 30% of speed of light
- The evolution of EW of the neutral absorption component (edge) and the ionized component (gabs), follow each other with a delay of the typical viscous timescale of 10 – 15 days. The evacuation of the inner accretion disk - a drop in the soft photon flux and an enhancement of hard flux.

THANKS！

Appendix

Data reduction

Swift/XRT

- Used *xrtpipeline*
- Source spectra : Circular region, R= 30 pixel

  (for pile up data annular region of outer

  circle 30 pixel and varying inner radius)
- Background : Annular region of 70-130 pixel radius
- Response file and ancillary response files are created
- Grouping : 20 photons per bin

NuSTAR

- Used *nupipeline*
- Source spectra : Circular region of 30 (35) pixel radius
- Background spectra : Circular region of 30 (35) pixel radius
- *NUPRODUCTS* task is used to generate science products such as light curves, energy spectra, response matrix files (RMFs) and auxiliary response files (ARFs) for both telescopes FPMA and FPMB.
- Grouping : 30 (50) photons per bin

Data reduction

NICER

- Used *nicerl2* task
- Applied barycenter corrections
- RMFs and ARFs are generated
- Background : generated using *nibackgen*
- Grouping : 25 photons per bin
- Systematics: 1.5 % (1%)

AstroSat

- Pile-up: annular extraction with Rin= 3 (2) arcmin and Rout=16 (15) arcmin.
- SXT: Sourc spectra, background and RMF files generated.
- ARF file generated using '*sxtARFModule*'.
- Grouping : 30 photons per bin
- LAXPC – *LaxpcSoftv3.4,* source spectrum, background and spectral response generated.
- Systematics of 2% - for SXT & LAXPC

Table 4.2: Wideband *NICER*-*NuSTAR* simultaneous pairs and *AstroSat* observations (highlighted in grey colour) using the model M1: `tbabs(thcomp×diskbb)edge×gabs` and `tbabs(thcomp×diskbb)gabs` respectively. The error values represent 90% confidence interval. The *NuSTAR* data on Epoch 8, 11 & 12 are not included here as no simultaneous *NICER* observations are available. The bolometric (0.5 – 100 keV) observed flux and estimated luminosity for each epoch is also shown.

Epoch	n_H ($\times10^{22}$ cm^{-2})	`diskbb`		`thcomp`			`edge` or `gauss`*		`gabs`			χ^2_{red}	F_{bol} ($\times10^{-8}$ erg cm^{-2} s^{-1})	L_{bol} (L_{Edd})
		T_{in} (keV)	norm ($\times10^3$)	Γ	k_BT_e (keV)	cov_frac ($\times10^{-2}$)	line E (keV)	D or σ (keV)	line E (keV)	σ (keV)	strength (keV)			
1	$0.470^{+0.002}_{-0.002}$	$1.272^{+0.002}_{-0.002}$	$7.96^{+0.05}_{-0.05}$	$2.44^{+0.06}_{-0.05}$	20^f	$2.3^{+0.2}_{-0.2}$	$7.16^{+0.05}_{-0.05}$	$0.04^{+0.01}_{-0.01}$	$10.0^{+0.1}_{-0.1}$	$1.60^{+0.09}_{-0.09}$	$0.84^{+0.08}_{-0.08}$	0.90	$27.64^{+0.04}_{-0.04}$	$1.52^{+0.14}_{-0.14}$
2	$0.458^{+0.002}_{-0.002}$	$1.159^{+0.002}_{-0.002}$	$6.07^{+0.04}_{-0.04}$	$2.0^{+0.1}_{-0.1}$	$11.6^{+3.9}_{-1.9}$	$0.9^{+0.2}_{-0.1}$	$7.19^{+0.07}_{-0.07}$	$0.03^{+0.01}_{-0.01}$	$9.9^{+0.1}_{-0.1}$	$1.65^{+0.07}_{-0.08}$	$1.2^{+0.1}_{-0.1}$	1.00	$17.22^{+0.02}_{-0.03}$	$0.95^{+0.09}_{-0.09}$
3	$0.52^{+0.02}_{-0.02}$	$0.99^{+0.01}_{-0.01}$	$15.4^{+1.5}_{-1.4}$	$1.84^{+0.14}_{-0.12}$	20^f	$0.39^{+0.07}_{-0.06}$	$6.77^{+0.15}_{-0.15}$	0.6^f	$7.35^{+0.34}_{-0.39}$	2^f	$1.73^{+0.47}_{-0.47}$	1.17	$19.5^{+0.1}_{-0.1}$	$1.07^{+0.001}_{-0.001}$
4	$0.461^{+0.002}_{-0.002}$	$1.094^{+0.002}_{-0.002}$	$5.82^{+0.05}_{-0.05}$	$2.2^{+0.1}_{-0.1}$	20^f	$0.3^{+0.1}_{-0.1}$	$7.27^{+0.07}_{-0.07}$	$0.05^{+0.01}_{-0.01}$	$10.4^{+0.1}_{-0.1}$	$1.94^{+0.08}_{-0.07}$	$2.2^{+0.2}_{-0.1}$	0.95	$12.38^{+0.02}_{-0.03}$	$0.68^{+0.06}_{-0.06}$
5	$0.458^{+0.002}_{-0.002}$	$1.050^{+0.002}_{-0.002}$	$5.77^{+0.04}_{-0.04}$	$2.3^{+0.2}_{-0.2}$	20^f	$0.2^{+0.1}_{-0.1}$	$7.28^{+0.05}_{-0.05}$	$0.06^{+0.01}_{-0.01}$	$10.7^{+0.1}_{-0.1}$	$1.97^{+0.08}_{-0.07}$	$2.7^{+0.2}_{-0.2}$	1.02	$10.10^{+0.01}_{-0.02}$	$0.56^{+0.05}_{-0.05}$
6	$0.50^{+0.02}_{-0.02}$	$0.97^{+0.02}_{-0.02}$	$12.1^{+1.5}_{-1.4}$	2.3^f	20^f	$0.3^{+0.02}_{-0.02}$	$6.77^{+0.18}_{-0.18}$	0.6^f	$9.05^{+0.51}_{-0.55}$	2.5^f	$2.27^{+0.66}_{-0.68}$	1.27	$13.9^{+0.06}_{-0.05}$	$0.76^{+0.001}_{-0.001}$
7	$0.54^{+0.01}_{-0.01}$	$0.98^{+0.01}_{-0.01}$	$7.64^{+0.33}_{-0.33}$	$2.26^{+0.06}_{-0.05}$	20^f	0.2^f	-	-	$10.7^{+0.2}_{-0.2}$	$1.46^{+0.24}_{-0.18}$	$1.56^{+0.25}_{-0.33}$	1.29	$9.36^{+0.21}_{-0.20}$	$0.51^{+0.004}_{-0.004}$
9	$0.451^{+0.003}_{-0.003}$	$0.966^{+0.002}_{-0.002}$	$5.60^{+0.05}_{-0.05}$	$2.6^{+0.5}_{-0.4}$	20^f	$0.1^{+0.2}_{-0.1}$	$7.44^{+0.08}_{-0.08}$	$0.08^{+0.02}_{-0.02}$	$10.5^{+0.2}_{-0.1}$	$2.02^{+0.09}_{-0.09}$	$3.3^{+0.3}_{-0.2}$	1.05	$6.88^{+0.02}_{-0.02}$	$0.38^{+0.04}_{-0.04}$
10	$0.53^{+0.01}_{-0.01}$	$0.96^{+0.01}_{-0.01}$	$5.63^{+0.35}_{-0.31}$	$1.92^{+0.30}_{-0.25}$	20^f	$0.11^{+0.05}_{-0.03}$	-	-	$10.1^{+0.2}_{-0.2}$	$1.56^{+0.20}_{-0.18}$	$2.13^{+0.39}_{-0.32}$	1.28	$7.59^{+0.04}_{-0.03}$	$0.40^{+0.001}_{-0.001}$
13	$0.52^{+0.01}_{-0.01}$	$0.91^{+0.01}_{-0.01}$	$7.48^{+0.24}_{-0.23}$	$1.77^{+0.03}_{-0.03}$	20^f	$0.12^{+0.05}_{-0.05}$	-	-	$9.42^{+0.27}_{-0.27}$	$0.75^{+0.30}_{-0.28}$	$0.47^{+0.13}_{-0.11}$	1.10	$6.59^{+0.06}_{-0.07}$	$0.36^{+0.002}_{-0.003}$
14	$0.48^{+0.01}_{-0.01}$	$0.91^{+0.01}_{-0.01}$	$7.92^{+0.58}_{-0.53}$	$1.94^{+0.02}_{-0.02}$	20^f	0.4^f	-	-	$10.7^{+0.24}_{-0.21}$	$1.34^{+0.18}_{-0.17}$	$1.47^{+0.18}_{-0.18}$	1.31	$6.22^{+1.89}_{-6.56}$	$0.34^{+0.08}_{-0.29}$
15	$0.465^{+0.004}_{-0.010}$	$0.904^{+0.030}_{-0.004}$	$6.10^{+0.09}_{-0.69}$	$2.09^{+0.04}_{-0.04}$	20^f	$1.6^{+0.1}_{-0.1}$	$7.31^{+0.08}_{-0.14}$	$0.10^{+0.05}_{-0.03}$	$9.6^{+0.3}_{-0.3}$	$2.1^{+1.2}_{-0.4}$	$1.1^{+1.1}_{-0.3}$	1.27	$5.66^{+0.02}_{-0.02}$	$0.31^{+0.03}_{-0.03}$
16	$0.471^{+0.002}_{-0.002}$	$0.897^{+0.002}_{-0.001}$	$6.22^{+0.05}_{-0.05}$	$2.04^{+0.04}_{-0.06}$	20^f	$1.6^{+0.1}_{-0.1}$	$7.35^{+0.06}_{-0.03}$	$0.12^{+0.02}_{-0.03}$	$9.4^{+0.4}_{-0.3}$	$1.5^{+0.4}_{-0.3}$	$0.5^{+0.1}_{-0.1}$	1.00	$5.39^{+0.01}_{-0.01}$	$0.30^{+0.03}_{-0.03}$

* `edge` is used for *NICER*-*NuSTAR* pairs whereas `gauss` component is used only for Epoch 3 & 6 of *AstroSat* data.

^{f} Frozen parameters

4U 1543-47

Table 4.3: Reflection modelling of *NICER*-*NuSTAR* simultaneous pairs and *AstroSat* observations (highlighted with grey colour) using the model `tbabs(diskbb+relxilllp)gabs`. The error values represent 90% confidence interval. The *NuSTAR* data on Epoch 8, 11 & 12 are not included here as no simultaneous *NICER* observations are available.

Epoch	n_H ($\times10^{22}$ cm^{-2})	diskbb T_{in} (keV)	diskbb norm ($\times10^3$)	relxilllp h (GM/c^2)	θ (deg)	Γ	$log\ \xi$ ($erg\ cm\ s^{-1}$)	A_{Fe} ($A_{Fe,\odot}$)	R_f	norm ($\times10^{-3}$)	gabs line E (keV)	σ (keV)	strength (keV)	χ^2_{red}
1	$0.49^{+0.01}_{-0.01}$	$1.276^{+0.001}_{-0.001}$	$6.31^{+0.03}_{-0.03}$	25.50^a	$32.7^{+3.4}_{-2.9}$	$2.81^{+0.03}_{-0.03}$	$3.58^{+0.09}_{-0.07}$	$8.5^{+1.2}_{-1.3}$	$1.4^{+0.1}_{-0.2}$	$282.7^{+84.3}_{-46.1}$	$9.9^{+0.1}_{-0.1}$	$2.05^{+0.1}_{-0.03}$	$1.1^{+0.1}_{-0.1}$	0.80
2	$0.70^{+0.04}_{-0.05}$	$1.151^{+0.006}_{-0.005}$	$6.3^{+0.2}_{-0.2}$	9.4^a	$36.3^{+1.6}_{-1.8}$	$2.94^{+0.04}_{-0.08}$	$3.65^{+0.05}_{-0.08}$	$7.7^{+1.2}_{-1.1}$	$3.5^{+0.9}_{-0.7}$	$200.4^{+47.8}_{-53.9}$	$9.8^{+0.1}_{-0.1}$	$1.94^{+0.09}_{-0.09}$	$1.3^{+0.2}_{-0.2}$	0.91
3	$0.46^{+0.02}_{-0.01}$	$1.01^{+0.006}_{-0.006}$	$11.7^{+0.76}_{-0.44}$	30^f	40^f	3.0^f	4.7^b	$9.37^b_{-0.40}$	$5.59^{+1.85}_{-3.48}$	$0.32^{+0.08}_{-0.08}$	$9.37^{+0.27}_{-0.13}$	$0.75^{+0.37}_{-0.64}$	$0.48^{+0.03}_{-0.19}$	1.37
4	$0.683^{+0.004}_{-0.03}$	$1.081^{+0.001}_{-0.001}$	$6.14^{+0.008}_{-0.04}$	$30.5^{+24.3}_{-2.0}$	$35.7^{+2.2}_{-2.7}$	$3.23^{+0.01}_{-0.06}$	$4.23^{+0.05}_{-0.04}$	$5.8^{+0.8}_{-0.7}$	10.0^a	$41.1^{+20.3}_{-2.0}$	$10.04^{+0.04}_{-0.07}$	$1.92^{+0.04}_{-0.06}$	$1.99^{+0.2}_{-0.08}$	0.83
5	$0.67^{+0.01}_{-0.03}$	$1.044^{+0.001}_{-0.001}$	$5.83^{+0.01}_{-0.04}$	$84.0^{+56.6}_{-18.3}$	$39.6^{+2.6}_{-3.1}$	$3.385^{+0.006}_{-0.05}$	4.7^b	$7.1^{+0.6}_{-0.7}$	10.0^a	$33.6^{+3.7}_{-2.5}$	$10.33^{+0.03}_{-0.03}$	$2.06^{+0.03}_{-0.05}$	$2.76^{+0.02}_{-0.06}$	0.83
6	$0.49^{+0.01}_{-0.02}$	$0.99^{+0.07}_{-0.01}$	$9.23^{+1.46}_{-0.19}$	100^f	40^f	3^f	$4.30^{+0.21}_{-0.21}$	10^b	7.18^a	$7.11^{+1.95}_{-4.1}$	$10.0^{+0.13}_{-0.14}$	$1.30^{+0.13}_{-0.13}$	$1.39^{+0.28}_{-0.11}$	1.30
7	$0.53^{+0.03}_{-0.01}$	$0.99^{+0.003}_{-0.003}$	$6.94^{+0.16}_{-0.27}$	8.26^a	40^f	$2.46^{+0.36}_{-0.25}$	$3.70^{+0.75}_{-0.68}$	10^b	9.99^a	$5.75^{+0.55}_{-0.69}$	$10.5^{+0.16}_{-0.14}$	$1.45^{+0.20}_{-0.17}$	$1.65^{+0.30}_{-0.25}$	1.44
9	$0.496^{+0.01}_{-0.007}$	$0.958^{+0.001}_{-0.001}$	$5.85^{+0.04}_{-0.04}$	40.29^a	40^f	$3.17^{+0.1}_{-0.06}$	4.7^b	10^b	10^f	$4.0^{+2.3}_{-1.0}$	$10.11^{+0.08}_{-0.08}$	$1.86^{+0.06}_{-0.06}$	$3.1^{+0.2}_{-0.2}$	1.10
10	$0.44^{+0.03}_{-0.01}$	$0.98^{+0.004}_{-0.004}$	$4.95^{+0.10}_{-0.90}$	70^f	40^f	$2.87^{+0.33}_{-0.24}$	4.7^b	10^b	8.10^a	$1.33^{+0.28}_{-0.12}$	$10.2^{+0.13}_{-0.12}$	$1.78^{+0.16}_{-0.19}$	$2.76^{+0.36}_{-0.38}$	1.19
13	$0.47^{+0.01}_{-0.01}$	$0.94^{+0.002}_{-0.003}$	$5.90^{+0.08}_{-0.09}$	44.3^a	40^f	2.25^f	$3.64^{+0.09}_{-0.18}$	$3.56^{+0.56}_{-0.46}$	8.10^a	$1.11^{+0.07}_{-0.16}$	$9.22^{+0.21}_{-0.18}$	$0.84^{+0.20}_{-0.21}$	$0.74^{+0.10}_{-0.13}$	1.11
14	$0.48^{+0.01}_{-0.01}$	$0.91^{+0.002}_{-0.002}$	$7.95^{+0.21}_{-0.12}$	6.69^a	40^f	$2.61^{+0.08}_{-0.19}$	$3.96^{+0.07}_{-0.26}$	10^b	10.6^a	$0.14^{+0.01}_{-0.01}$	$10.1^{+0.13}_{-0.13}$	$1.03^{+0.12}_{-0.13}$	$1.25^{+0.14}_{-0.14}$	1.24
15	$0.475^{+0.004}_{-0.003}$	$0.906^{+0.001}_{-0.001}$	$5.91^{+0.04}_{-0.04}$	33.74^a	$38.0^{+8.5}_{-4.4}$	$2.07^{+0.06}_{-0.06}$	$2.7^{+0.1}_{-0.3}$	10.0^b	$0.9^{+0.2}_{-0.2}$	$4.9^{+1.5}_{-0.7}$	$9.1^{+0.1}_{-0.1}$	$1.5^{+0.1}_{-0.2}$	$1.0^{+0.1}_{-0.1}$	1.12
16	$0.482^{+0.004}_{-0.004}$	$0.904^{+0.001}_{-0.001}$	$5.63^{+0.05}_{-0.05}$	50.01^a	$36.7^{+9.4}_{-5.5}$	$2.05^{+0.05}_{-0.05}$	$3.7^{+0.1}_{-0.2}$	10.0^b	$0.9^{+0.2}_{-0.1}$	$4.2^{+0.8}_{-0.6}$	$8.7^{+0.1}_{-0.1}$	$1.49^{+0.08}_{-0.08}$	$1.2^{+0.2}_{-0.2}$	0.87

[a] Parameter uncertainty can't be estimated.
[b] Parameter hits the boundary.
[f] Frozen parameters.

Table 5.1: Parameters of phenomenological spectral modelling of *NuSTAR* using the model `tbabs(thcomp×diskbb)edge×gabs` (M1). Errors are in 90% confidence intervals.

Epoch	diskbb		thcomp			edge		gabs			χ^2_{red}
	T_{in} (keV)	norm ($\times 10^3$)	Γ	$k_B T_e$ (keV)	cov_frac ($\times 10^{-2}$)	line E (keV)	D (keV)	line E (keV)	σ (keV)	strength (keV)	
1	$1.238^{+0.005}_{-0.004}$	$3.81^{+0.06}_{-0.08}$	$2.73^{+0.06}_{-0.06}$	150.00^a	$0.088^{+0.007}_{-0.032}$	$7.2^{+0.1}_{-0.1}$	$0.04^{+0.01}_{-0.01}$	$10.0^{+0.2}_{-0.1}$	$1.3^{+0.2}_{-0.1}$	$0.48^{+0.10}_{-0.07}$	1.17
2	$1.129^{+0.003}_{-0.001}$	$3.58^{+0.05}_{-0.05}$	$2.3^{+0.1}_{-0.1}$	24.53^a	$0.026^{+0.017}_{-0.005}$	$7.20^{+0.07}_{-0.07}$	$0.05^{+0.01}_{-0.01}$	$9.82^{+0.07}_{-0.09}$	$1.27^{+0.09}_{-0.08}$	$0.68^{+0.08}_{-0.07}$	1.14
4	$1.055^{+0.003}_{-0.002}$	$3.58^{+0.05}_{-0.06}$	$2.4^{+0.2}_{-0.3}$	24.75^a	$0.008^{+0.007}_{-0.003}$	$7.23^{+0.05}_{-0.05}$	$0.08^{+0.01}_{-0.01}$	$10.06^{+0.09}_{-0.09}$	$1.32^{+0.09}_{-0.09}$	$1.0^{+0.1}_{-0.1}$	1.09
5	$1.024^{+0.004}_{-0.004}$	$3.27^{+0.07}_{-0.08}$	$2.0^{+0.6}_{-0.9}$	9.98^a	$0.002^{+0.005}_{-0.002}$	$7.28^{+0.06}_{-0.06}$	$0.09^{+0.02}_{-0.02}$	$10.3^{+0.2}_{-0.2}$	$1.5^{+0.1}_{-0.1}$	$1.5^{+0.2}_{-0.3}$	1.07
8	$0.952^{+0.005}_{-0.004}$	$3.31^{+0.09}_{-0.10}$	$2.1^{+0.3}_{-0.3}$	7.53^a	$0.002^{+0.001}_{-0.001}$	$7.27^{+0.06}_{-0.06}$	$0.10^{+0.02}_{-0.02}$	$10.1^{+0.2}_{-0.1}$	$1.5^{+0.1}_{-0.1}$	$1.8^{+0.3}_{-0.2}$	1.13
9	$0.940^{+0.004}_{-0.004}$	$3.29^{+0.08}_{-0.09}$	$2.7^{+0.4}_{-0.5}$	150.00^a	$0.004^{+0.003}_{-0.003}$	$7.36^{+0.07}_{-0.07}$	$0.10^{+0.02}_{-0.02}$	$10.2^{+0.1}_{-0.1}$	$1.6^{+0.1}_{-0.1}$	$2.0^{+0.3}_{-0.2}$	1.04
11	$0.921^{+0.002}_{-0.002}$	$3.27^{+0.05}_{-0.06}$	$2.00^{+0.10}_{-0.08}$	21.04^a	$0.016^{+0.009}_{-0.002}$	$7.20^{+0.04}_{-0.04}$	$0.11^{+0.02}_{-0.02}$	$9.4^{+0.1}_{-0.1}$	$1.1^{+0.1}_{-0.1}$	$0.7^{+0.1}_{-0.1}$	1.03
12	$0.920^{+0.004}_{-0.004}$	$2.94^{+0.08}_{-0.08}$	$2.20^{+0.09}_{-0.07}$	19.90^a	$0.087^{+0.020}_{-0.010}$	$7.27^{+0.09}_{-0.09}$	$0.10^{+0.02}_{-0.02}$	$9.5^{+0.4}_{-0.4}$	$1.0^{+0.3}_{-0.3}$	$0.17^{+0.06}_{-0.07}$	1.06
15	$0.901^{+0.002}_{-0.003}$	$3.11^{+0.06}_{-0.06}$	$1.98^{+0.08}_{-0.07}$	19.76^a	$0.026^{+0.007}_{-0.003}$	$7.07^{+0.09}_{-0.04}$	$0.07^{+0.02}_{-0.02}$	$9.2^{+0.1}_{-0.1}$	$1.1^{+0.1}_{-0.1}$	$0.54^{+0.11}_{-0.09}$	1.13
16	$0.897^{+0.002}_{-0.003}$	$3.05^{+0.06}_{-0.07}$	$1.92^{+0.08}_{-0.06}$	15.01^a	$0.026^{+0.004}_{-0.002}$	$7.3^{+0.1}_{-0.1}$	$0.09^{+0.03}_{-0.03}$	$9.0^{+0.3}_{-0.3}$	$1.0^{+0.2}_{-0.2}$	$0.33^{+0.11}_{-0.09}$	1.05

[a] Parameter uncertainty can't be estimated.

Table 5.2: Parameters of the reflection modelling of *NuSTAR* using the model `tbabs(diskbb+relxilllp)gabs` (M2). Errors are in 90% confidence intervals.

Epoch	`diskbb`		`relxilllp`							`gabs`			χ^2_{red}
	T_{in} (keV)	$norm$ $(\times 10^3)$	h (GM/c^2)	θ (deg)	Γ	$log\ \xi$ $(erg\ cm/s)$	A_{Fe} $(A_{Fe,\odot})$	R_f	$norm$ $(\times 10^{-3})$	$line\ E$ (keV)	σ (keV)	$strength$ (keV)	
1	$1.24^{+0.01}_{-0.01}$	$7.2^{+0.3}_{-0.3}$	$40.03^{+2.5}_{-2.3}$	$25.8^{+6.3}_{-8.4}$	$2.72^{+0.09}_{-0.09}$	$4.0^{+0.5}_{-0.5}$	10.0^{b}	$0.4^{+0.4}_{-0.1}$	$0.23^{+0.08}_{-0.07}$	$9.7^{+0.2}_{-0.2}$	$1.6^{+0.3}_{-0.2}$	$0.6^{+0.2}_{-0.1}$	1.16
2	$1.112^{+0.002}_{-0.002}$	$7.44^{+0.05}_{-0.05}$	$9.4^{+4.6}_{-3.7}$	$28.9^{+3.6}_{-3.7}$	$2.60^{+0.1}_{-0.05}$	$4.1^{+0.2}_{-0.2}$	10^{b}	$1.2^{+0.3}_{-0.2}$	$8.16^{+0.08}_{-0.02}$	$9.4^{+0.1}_{-0.1}$	$1.4^{+0.1}_{-0.1}$	$0.59^{+0.08}_{-0.09}$	1.02
4	$1.058^{+0.003}_{-0.003}$	$6.84^{+0.089}_{-0.09}$	$16.62^{+13.8}_{-7.6}$	$33.6^{+2.3}_{-1.8}$	3.21^{a}	4.52^{a}	10.0^{b}	$4.8^{+2.3}_{-1.7}$	$0.1^{+0.1}_{-0.05}$	$9.8^{+0.1}_{-0.2}$	$1.8^{+0.2}_{-0.2}$	$1.5^{+0.3}_{-0.3}$	1.10
5	$1.035^{+0.001}_{-0.001}$	$6.09^{+0.2}_{-0.01}$	$32.42^{+8.7}_{-5.6}$	$34.49^{+2.8}_{-2.7}$	$3.37^{+0.01}_{-0.1}$	4.7^{b}	$9.13^{+0.8}_{-0.7}$	34.06^{a}	$0.0127^{+0.0007}_{-0.0007}$	$10.03^{+0.04}_{-0.04}$	$1.95^{+0.03}_{-0.03}$	$2.29^{+0.04}_{-0.04}$	1.03
8	$0.962^{+0.002}_{-0.001}$	$6.20^{+0.08}_{-0.04}$	$41.9^{+32.3}_{-12.9}$	$37.3^{+3.1}_{-5.2}$	$3.37^{+0.02}_{-0.19}$	4.7^{b}	10.0^{b}	11.86^{a}	$0.013^{+0.006}_{-0.001}$	$9.95^{+0.14}_{-0.07}$	$1.76^{+0.03}_{-0.06}$	$2.53^{+0.06}_{-0.05}$	1.17
9	$0.949^{+0.001}_{-0.002}$	$6.15^{+0.01}_{-0.1}$	81.35^{a}	$43.5^{+6.2}_{-6.3}$	$3.16^{+0.03}_{-0.07}$	4.7^{b}	10.0^{b}	14.58^{a}	$0.0031^{+0.0003}_{-0.0003}$	$9.94^{+0.03}_{-0.09}$	$1.72^{+0.02}_{-0.03}$	$2.54^{+0.04}_{-0.08}$	1.12
11	$0.923^{+0.002}_{-0.002}$	$6.4^{+0.1}_{-0.1}$	22.45^{a}	$39.5^{+6.1}_{-2.8}$	$2.39^{+0.1}_{-0.04}$	$2.6^{+0.2}_{-0.4}$	10.0^{b}	$2.6^{+0.4}_{-0.4}$	$0.007^{+0.006}_{-0.002}$	$9.22^{+0.1}_{-0.08}$	$1.48^{+0.1}_{-0.05}$	$1.2^{+0.2}_{-0.1}$	1.04
12	$0.90^{+0.01}_{-0.01}$	$6.3^{+0.5}_{-0.4}$	9.04^{a}	$30.1^{+4.1}_{-4.4}$	$2.24^{+0.06}_{-0.04}$	$3.6^{+0.4}_{-0.3}$	8.90^{a}	$0.5^{+0.2}_{-0.2}$	$0.03^{+0.03}_{-0.01}$	$8.6^{+0.3}_{-0.3}$	$1.3^{+0.3}_{-0.3}$	$0.4^{+0.3}_{-0.2}$	1.01
15	$0.903^{+0.005}_{-0.005}$	$6.0^{+0.2}_{-0.2}$	32.3^{a}	21.05^{a}	$1.96^{+0.06}_{-0.08}$	$3.3^{+0.3}_{-0.3}$	10.0^{b}	$0.4^{+0.3}_{-0.2}$	$0.004^{+0.002}_{-0.001}$	$9.06^{+0.09}_{-0.13}$	$1.3^{+0.1}_{-0.1}$	$0.9^{+0.2}_{-0.2}$	1.10
16	$0.898^{+0.01}_{-0.008}$	$5.9^{+0.3}_{-0.2}$	26.0^{a}	$32.8^{+27}_{-6.8}$	$2.0^{+0.1}_{-0.1}$	$3.3^{+0.4}_{-0.6}$	10.0^{b}	$0.6^{+0.3}_{-0.2}$	$0.005^{+0.004}_{-0.001}$	$8.8^{+0.1}_{-0.1}$	$1.3^{+0.2}_{-0.2}$	$0.9^{+0.3}_{-0.3}$	1.04

[a] Parameter uncertainty can't be estimated.
[b] Parameter hits the boundary.